CHAPTER 8

A TEST CASE STUDY OF PEC SOLAR CELLS USING n-TYPE NATURAL MoS_2 SINGLE CRYSTALS

CONTENTS

8.1 Introduction

Photoelectrochemical (PEC) systems for converting radiant energy into electrical/ chemical energy are midway between solid state photovoltaic devices and electrochemical cells. On one hand this creates a new material problem, such as photocorrosion of the photoactive materials, while on the other hand the demand for lattice match is completely replaced by that of rapid kinetics of the electrochemical reaction occuring in the cell. The layer type transition metal dichalcogenides like MoS_2 and $MoSe_2$ have extensive metal to metal bonding and it allows valence changes which are affected by d-d transitions and thus not endangering MO-X bonds. Therefore, they have promising stability.

As molybdenum disulfide crystals are available in natural and synthetic forms, it is interesting to study both of them from photoelectrochemical properties point of view. Naturally occouring samples of MoS_2 are observed to be p-type, n-type or intrinsic. Tributsch et al /1/ have studied the PEC behaviour of natural MoS_2 single crystals in $Fe^{2+/3+}$ solution. They have reported exhaustive results for natural p-MoS_2 crystals. Influence of crystal surface orientation on redox reactions at semiconducting n-MoS_2 has also been

examined by Ahmed and Gerischer /2/. These results have shown that PEC behaviour of n-type natural MoS_2 is interesting. And also for the verification of the validity of the results obtained by using the single crystals of tungsten sulfo-selenide in the fabrication of PEC solar cells (which will be discussed in the following chapters) as a test case study, we have striven in the present work to fabricate PEC solar cells by employing the single crystals of n-type MoS_2 which are available abundantly in nature.

In this chapter, it should be mentioned that for the fabricated solar cells in the above manner, estimation of ideality factor, measurements of flat band potential and temperature effect have not been reported so far. This was also a cardinal interest of this study.

8.2 Experimental

Naturally available n-type samples of molybdenite, MoS_2, were used in the present work. The semiconducting nature was confirmed by Hot-probe method and from Mott-Schottky plot. Photoelectrochemical solar cells were fabricated using the single crystals of MoS_2 as photoelectrode (photoanode) and platinum grid of area 1 cm^2 as counter electrode. The electrodes were immersed in the aqueous iodide solution having concentration

equal to 0.025 MI_2 + 1.9 M NaI + 0.5 M Na_2SO_4 + 0.5 M H_2SO_4.
The schematic diagram of experimental set up of PEC cell is displayed in Fig. 8.1. The crystal surface (basal) was connected to a copper wire with silver paste and the crystal was mounted on a glass plate by applying clear epoxy resin along the boundary to insulate the back surface and the connecting wire from the electrolyte. In this way, the semiconductor photoelectrode was prepared. The exposed surface areas of semiconducting crystals were kept about 0.013, 0.019, 0.052 and 0.127 (all in cm^2). The impedance measurements and dark I-V characteristics were obtained while keeping the cell well protected from light. The solution used was with PH = 7 in the above concentration. A diagram representing the experimental set up of PEC cell for impedance (capacitive) measurements is given in Fig. 8.2 and circuit diagram for dark I-V characteristics and illuminated I-V characteristics are presented in chapter 9.

The crystal surface of photoelectrode was illuminated (except in the study of dark I-V and flat band potential measurements) by an incandescent 6V - 15 W microscope lamp, for solar conversion measurements. The intensity of illumination at the crystal surface was measured with Suryamapi (Central Electronics Ltd. (CEL) Co.).

Photovoltages and photocurrents were recorded by digital multimeter and Philips meter VASL (PM 2505) respectively. Iodide electrolyte was prepared from A. R. grade chemicals in double distilled water. To examine the temperature dependence, a magnetic stirrer was used for establishing uniform temperature of electrolyte. Capacitance observations were taken with the help of VLCR-23 meter. A saturated calomel reference electrode was employed to measure voltage (potential) applied to semiconductor electrode.

8.3 Results and Discussion

When the semiconductor electrolyte junction is illuminated with light having energy greater than bandgap energy of semiconductor, electron hole pairs are produced in the depletion region of junction and charge separation takes place due to the local field present at the interface. When a counter electrode is immersed in the electrolyte and connected to the semiconductor, the photogenerated electron moves into the bulk of the semiconductor and through external circuit it reaches the counter electrode to reduce the oxidised species in the electrolyte. The hole is pushed to the electrode surface where it oxidizes the reduced species in the electrolyte.

Dark current-voltage characteristics for natural n-type MoS_2 is shown in Fig. 8.3(a) (Details of the procedure to take dark I-V is explained in chapter 9). In a Schottky barrier the dark current is given by the relation

$$I = I_0 \exp(eV/nKT) \qquad (8.1)$$

where V is applied bias voltage and n is the slope of ln I - V plot as

$$n = \frac{e}{KT}\left(\frac{dV}{d\ln I}\right) \qquad (8.2)$$

The linear nature of the graph of ln I versus V can be seen from Fig. 8.3(b). The slope n given by above relation is known as junction ideality factor. Observed values of n are found to be more than one i.e. 1.6 (from Fig. 8.3(b)). Higher values of n indicate recombination processes in space charge layer. Tunneling currents and interfacial layers can result in higher values of n equal to or greater than 2.

To determine the energetic location of the valence and conduction band edges as well as flat band potential, the space charge capacitance measurements

were undertaken. Capacitance data from well behaved electrode were used to obtain Mott-Schottky plot ($\frac{1}{C^2}$ versus V_{sce}). The use of such plots is universely accepted as the best way to determine the flat band potential /3/. The above plot showed good straight line over limited potential range (Fig. 8.4). The intercept of this line enabled us to estimate the value of flat band potential V_{fb} which is 0.20 V (voltage with respect to calomel electrode) in the present case. Wieting /4/ has reported the carrier concentration at room temperature about 2×10^{17} cm^{-3} for natural MoS_2 crystals. This value is in almost agreement with the present value evaluated in the following way. From the slope of the Mott-Schottky plot, the donor density $N_D = 4.158 \times 10^{17}$ cm^{-3} was calculated using the following relations.

$$\frac{1}{C^2} = \frac{2}{\epsilon \epsilon_0 \cdot N_D} \left(|V_{sce}| - \frac{kT}{e} \right) \qquad (8.3(a))$$

$$N_D = 2 \left[e \epsilon \epsilon_0 \, (slope) \right]^{-1} \qquad (8.3(b))$$

where ϵ (=7·34) is the dielectric constant of semiconductor due to Evans et al /5/ and ϵ_0 the permittivity of free space. Tributsch et al /6/ have reported the band gap for n-MoS_2 to be 1.78 eV. From this result and the above data, we could estimate the positions of valence band and the conduction band. It has also been predicted /7/ that a difference of 0.2 eV between the Fermi level and the edge of conduction band exist in the case of n-MoS_2 crystal. This locates the position of conduction band (E_c) at 0 V_{sce}. It is evident that below this level at a position of 1.78 V_{sce}, we get the valence band edge (E_v). Thus, we obtain a complete energy level diagram for the system of semiconductor-electrolyte -metal at equilibrium in dark. The corresponding positions of valence band, conduction band and Fermi level so obtained are shown in Fig. 8.5. This suggests that the redox couple with potential V_{redox} within the gap 0 and 1.78 V_{sce} should be appropriate for PEC cells with natural n-type MoS_2. In the present case the redox couple is 0.3 V_{sce}. However from Fig. 8.5 it was found that the photovoltage did not obey equation

$$V_{oc} = \left| E_F - E_{redox} \right| \qquad (8.3(a))$$

Bard et al /8/ and Wrighton et al /9/ concluded that the non-validity of above equation is due to the effect that surface states pin the fermi level.

I-V characteristics of the PEC solar cell under different levels of illumination are shown in Fig. 8.6(a). Tributsch /1/ has pointed out the square root dependence of photocurrent (I_{sc}) on the light intensity (I_L)

$$I_{sc} \sim I_L^{\frac{1}{2}} \qquad (8.4)$$

According to Schottky barrier model, open circuit voltage is given by

$$V_{oc} = \frac{nKT}{e} \ln \left(\frac{I_{sc}}{I_o} \right) \qquad (8.5)$$

where I_o is reverse saturation current and I_{sc} is short circuit current.

From square root dependance of photo-current, the open circuit voltage can be expressed as

$$V_{oc} = \frac{nKT}{e} \ln \left(\frac{C\, I_L^{\frac{1}{2}}}{I_o} \right) \qquad (8.6)$$

Here C is a constant. The equation (8.6) indicates that V_{oc} is logarithmic function of light

intensity. It is evident from Fig. 8.6(b) that open circuit voltage (V_{oc}) and short circuit current density (J_{sc}) increases as intensity increases. Variation of power conversion efficiency with respect to intensity of illumination is exhibited in Fig. 8.6(c). From this figure it can be seen that the efficiency of the cell shows increasing trend as the intensity is increased.

The effect of temperature on V_{oc} and I_{sc} can be judged from Fig. 8.7(a). Similar effect on the efficiency is represented in Fig. 8.7(b). Basically, the principal mechanism for temperature dependent effects is to produce shift in the energy levels of semiconductor and electrolyte. It also produces changes in the electrochemical rates /10/. Shifts in energy level positions cause two effects which are (i) changes in band gap and thus optical response and (ii) changes in open circuit voltage. The open circuit voltage for PEC cell depends on the difference between the flat band potential and the relevent redox potential. The factors affecting flat band potential has shown that it may be expressed /10/ as follows,

$$V_{fb} = E_A - E_0 - \Delta F_c - \Delta p_x \qquad (8.7)$$

where E_A is semiconductor electron affinity measured from vacuum level. E_e is the reference electrode potential measured from the vacuum level, ΔF_c is the difference between the semiconductor Fermi level and the conduction band for n-type electrodes and Δpx is the potential drop due to ions absorbed on semiconductor surface. All the factors in the above expression are temperature dependent which give resultant effect in V_{fb}. It is noted here that a quantitative analysis of this dependency could have explained the corresponding variation in V_{oc}, I_{sc} and the efficiency of the cell. However, from figures 8.7(a) and 8.7(b) it can be inferred that broadly as the temperature increases, V_{oc} decreases while I_{sc} and efficiency (n), initially increases up to some maximum value and then decreases.

According to Butler /11/, the total photo-current is consisting of two components which are :

(1) from carriers generated in the bulk which diffuse into the depletion layer before recombining and (11) from carriers generated in the depletion layer. This photocurrent is expressed as

$$J = e\phi_0 \left[1 - \frac{\exp -\{V_0(V - V_{fb})^{\frac{1}{2}}\}}{1 - \alpha L_p}\right] \qquad (8.8)$$

where ϕ_o is the photon flux, α is optical absorption coefficient, W_o the depletion layer thickness for one volt across it and L_p is the hole diffusion length. This describes the dependence of photocurrent on the various parameters of semiconductor (ϵ_o, N_D , α, L_p and V_{fb}). From the present results (Figs. 8.7(a) and 8.7(b)) we may mention that due to last equation, flat band potential and diffusion length must be decreasing (after attaining the optimum values) with the rise in temperature.

The variation of efficiency for the cell while changing concentration of I_2 molecule into the electrolyte is shown in Fig. 8.8. Maximum open circuit voltage is determined from the difference between conduction band edge and the redox potential. Butler /10/ has stated that the redox potentials are generally known as function of electrolyte composition. Depending on change in redox potential by addition of molecular I_2, the open circuit voltage and photocurrent changes and maximum power is obtained at particular concentration of redox couple. This situation gives highest efficiency as shown in Fig. 8.8.

Stability of photoelectrode means ageing effect. This is shown in Fig. 8.9. It indicates a slight decrease in photocurrent but almost stable photocurrent was

observed for several hours. Still however, it should be noted that in the present case, the natural n-MoS_2 did not turn out to be sufficiently stable for long duration against oxidation by its reaction product.

8.4 Conclusions

In the present test case study it has been found that the low energy conversion efficiencies of the cell is the usual result associated with PEC systems in general and it is still to be tackled. It was noticed that electrical power conversion efficiencies vary from 0.15 % to 0.95 %. It was also observed during the course of work that fill factor and efficiencies of the cells vary from sample to sample. This may be due to the presence of usual impurities in the natural crystals.

References

/1/ Tributsch, H. (1977).
Ber. Bunsen. Phy. Chem. 81 , No. 4, 361.

/2/ Ahmed, S. M. and Gerischer, H. (1979).
Electrochemica Acta 24 , 705.

/3/ Kautek, W. and Gerischer, H. (1980).
Ber. Bunsen. Phys. Chem. 84 , 645.

/4/ Wieting, T. J. (1970).
J. Phys. Chem. Solids. 31 , 2134.

/5/ Evans, B. L. (1965).
Proc. Roy. Soc. A 284 , 418.

/6/ Tributsch, H. (1980).
J. Electrochem. Soc. 127 , 2471.

/7/ Ahmed, S. M. (1982).
Electrochemica Acta. 27 , 707.

/8/ Bard, A. J. (1980).
J. Am. Chem. Soc. 102 , 3673.

/9/ Wrighton, M. S. (1980).
J. Am. Chem. Soc. 102 , 6964.

/10/ Butler, M. A. (1980).
J. Material Sci. 15, 1.

/11/ Butler, M. A. (1977).
J. Appl. Phys. 48 , 1914.

Captions to the Figures

Fig. 8.1 PEC solar cell using n-type natural MoS_2 single crystal as photoelectrode and platinum as counter electrode.

1. Semiconducting crystal
2. Incident light
3. Electrolyte
4. Platinum grid

Fig. 8.2 Schematic diagram of experimental set up of PEC cell for impedance measurement.

Fig. 8.3(a) Dark current-voltage characteristics for natural n-MoS_2 in aqueous iodide solution.

Fig. 8.3(b) Plot of logarithm of dark current (log I) versus applied voltage (V_{app}).

Fig. 8.4 Plot of reciprocal of capacitance square ($\frac{1}{C^2}$) versus applied voltage with respect to saturated calomel electrode V_{sce} (Mott Schottky plot).

Fig. 8.5 Energy level diagram of the system on natural n-type MoS_2/electrolyte/ platinum electrode at equilibrium in dark.

Fig. 8.6(a) Current density (J) - Voltage (V) characteristics of PEC solar cell under different levels of illumination.

Fig. 8.6(b) Variation of open circuit voltage (V_{oc}) and short circuit current density (J_{sc}) with different levels of illumination.

Fig. 8.6(c) Solar to electrical power conversion efficiency as a function of light intensity.

Fig. 8.7(a) Effect of temperature on open circuit photovoltage (V_{oc}) and short circuit photocurrent (I_{sc}).

Fig. 8.7(b) Variation of power conversion efficiency (n) with temperature.

Fig. 8.8 Effect of concentration of I_2 on power conversion efficiency (n).

Fig. 8.9 Stability of a solar cell as a function of time in hours.

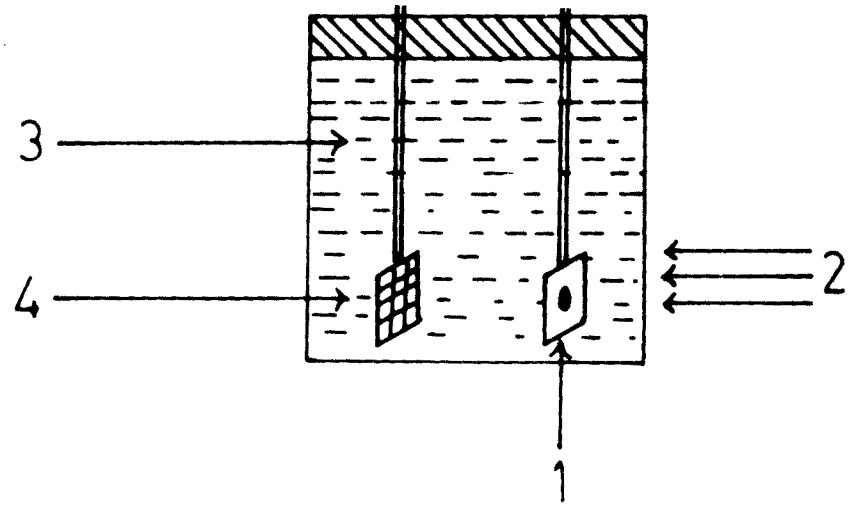

Fig. 8.1

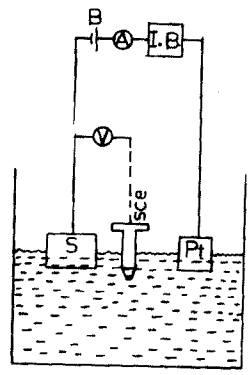

(1) S — SAMPLE
(2) Pt — PLATINUM GRID
(3) SCE
(4) V — VOLTMETER
(5) B — BATTERY
(6) A — AMMETER
(7) IB — IMPEDANCE BRIDGE.

Fig. 8.2

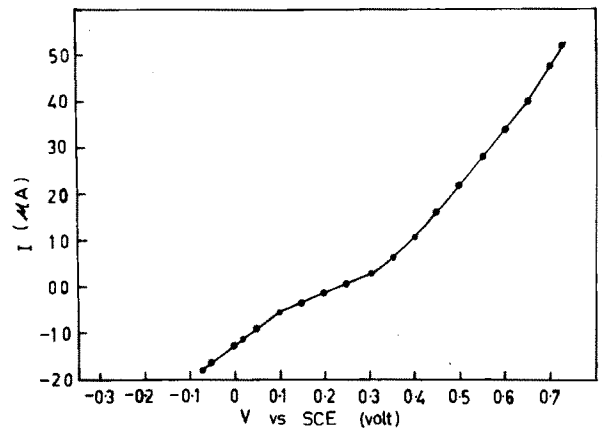

Fig. 8.3(a)

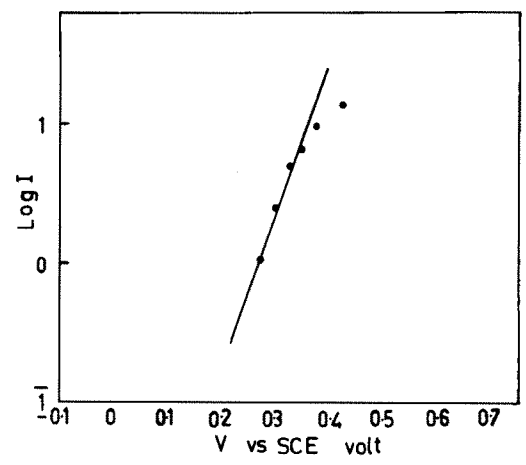

Fig. 8.3(b)

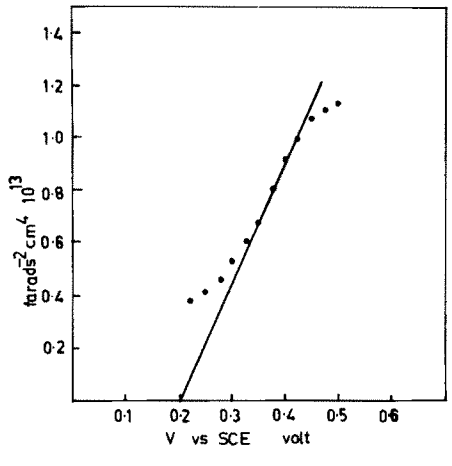

Fig. 8.4

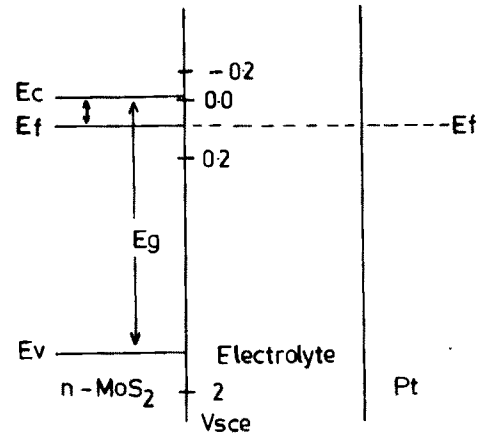

Fig. 8.5

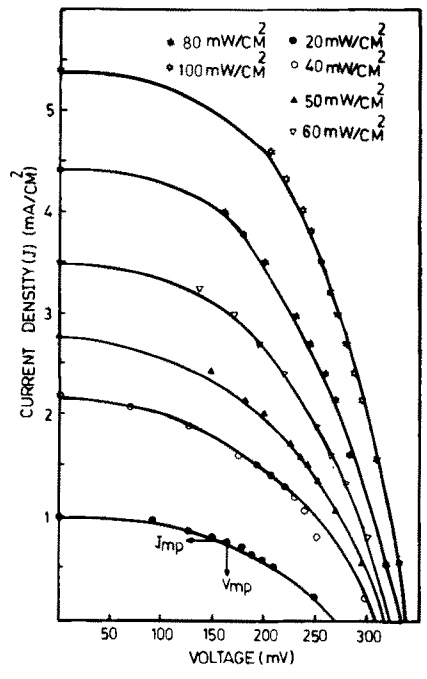

Fig. 8.6(a)

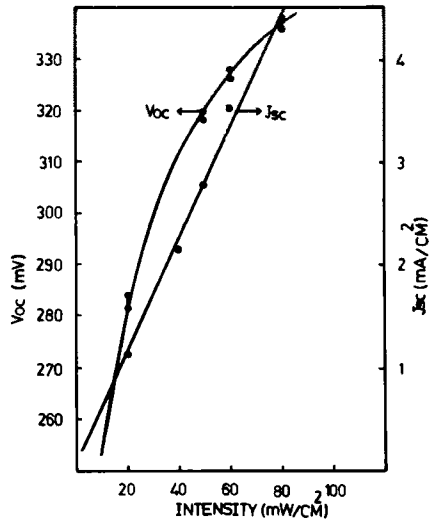

Fig. 8.6(b)

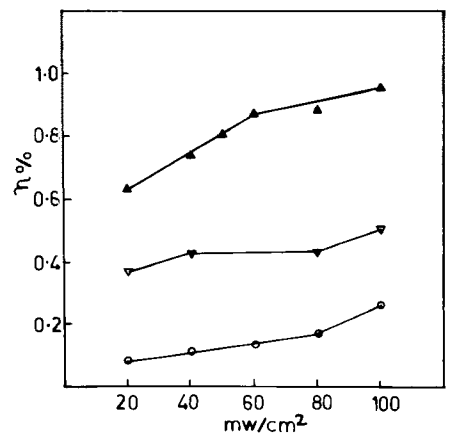

Fig. 8.6(c)

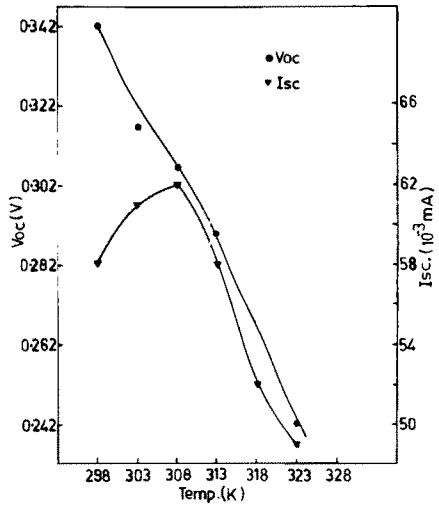

Fig. 8.7(a)

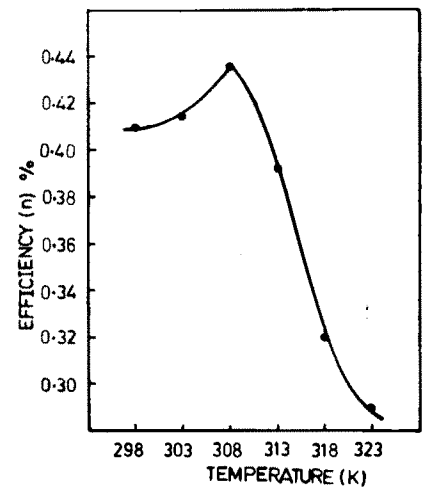

Fig. 8.7(b)

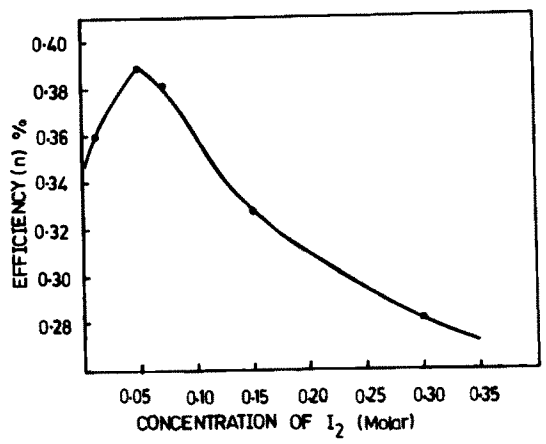
0·40
0·38
0·36
0·34
0·32
0·30
0·28
EFFICIENCY (η) %
0·05
0·10
0·15
0·20
0·25
0·30
0·35
CONCENTRATION OF I_2 (Molar)

Fig. 8.8

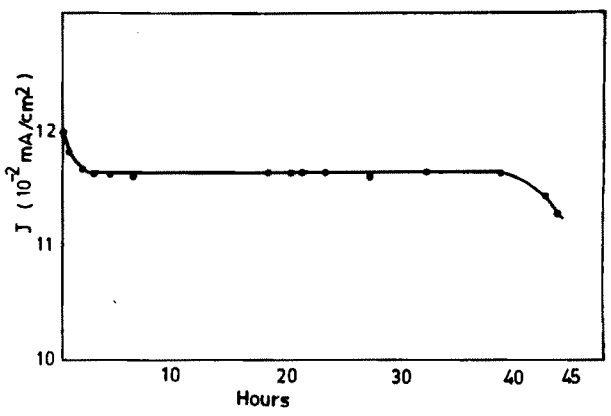
J (10^{-2} mA/cm^2)
12
11
10
10
20
30
40
45
Hours

Fig. 8.9